



A chance-constrained programming level set method for longitudinal segmentation of lung tumors in CT and CT/PET images

Méthode par ensembles de niveaux avec contrainte stochastique pour la segmentation longitudinale de tumeurs du poumon en imagerie par TDM et TDM/TEP

Youssef Rouchdy
Isabelle Bloch

2011D004

avril 2011

Département Traitement du Signal et des Images
Groupe TII : Traitement et Interprétation des Images

A Chance-Constrained Programming Level Set method for longitudinal segmentation of lung tumors in CT and CT/PET images

Méthode par ensembles de niveaux avec contrainte stochastique pour la segmentation longitudinale de tumeurs du poumon en imagerie par TDM et TDM/TEP

Youssef Rouchdy and Isabelle Bloch

Institut Telecom, Telecom ParisTech, CNRS LTCI
46 rue Barrault - 75013 Paris, France
youssef.rouchdy@gmail.com, isabelle.bloch@telecom-paristech.fr

Abstract. This paper presents a novel stochastic level set method for the longitudinal tracking of lung tumors in computed tomography (CT) and CT/PET images. The proposed model addresses the limitations of registration-based and segmentation-based methods for longitudinal tumor tracking. It combines the advantages of each approach using a new probabilistic framework, namely chance-constrained programming (CCP). Lung tumors can shrink or grow over time, which can be reflected in large changes of shape, appearance and volume in CT images. Traditional level set methods with a priori knowledge about shape are not suitable since the tumors are undergoing random and large changes in shape. Our CCP level set model allows us to introduce a flexible prior to track structures with a highly variable shape by permitting a constraint violation up to a specified probability level. The chance constraints are computed from two given points by the user or from segmented tumors from a reference image. The reference image can be one of the images studied or an external template. We present a numerical scheme to approximate the solution of the proposed model and apply it to track lung tumors in CT and CT/PET data. Finally we compare our approach with a Bayesian level set. The CCP level set model gives the best results: it is more coherent with the manual segmentation.

Keywords: Level set methods, stochastic level set methods, chance constraints, image segmentation, longitudinal tumor tracking in CT and CT/PET images.

Résumé : Cet article présente une méthode originale pour la segmentation longitudinale de tumeurs du poumon en imagerie médicale par

émission de positons (TEP) et tomodensitométrie (TDM). Le modèle proposé aborde les limitations des méthodes de segmentation et de recalage pour le suivi de tumeurs. Notre modèle utilise un formalisme probabiliste original, appelé modèle de contraintes fortuites (CCP). Les tumeurs du poumon sont soumises à des grandes déformations au cours de la respiration, et cela se traduit par des grands changements de forme et d'apparence aléatoires dans les images TDM. Les méthodes par ensembles de niveaux traditionnelles avec un a priori de forme ne permettent pas de gérer ce genre de changements. Notre modèle CCP introduit des contraintes souples sur l'évolution des ensembles de niveaux en permettant des violations des contraintes de forme imposées jusqu'à un niveau de probabilité prédéfini par l'utilisateur. Les contraintes CCP sont calculées à partir de deux points donnés par l'utilisateur, le premier point étant situé à l'intérieur de la tumeur et le second sur le bord de la tumeur. Ces points sont donnés sur une image de référence, typiquement l'image acquise à la première date. Ces deux points peuvent être remplacés par une segmentation manuelle de la tumeur dans l'image de référence. Nous présentons un schéma numérique pour estimer la solution du modèle proposé. Nous appliquons notre méthode à la segmentation longitudinale de tumeurs en imagerie TDM et TDM/TEP. Les résultats obtenus avec notre modèle sont meilleurs que ceux obtenus par un modèle bayésien. En effet les résultats obtenus par CCP sont plus cohérents avec la segmentation manuelle.

Mots clés : Ensembles de niveaux, méthodes stochastiques, contraintes fortuites, segmentation d'images, suivi longitudinal de tumeurs en TDM et TDM/TEP.

1 Introduction

In this work we aim to estimate longitudinal tumor volumes to compute accurately the change in tumor volume. These volumes can be used as tumor indicators or to compute a local SUV measure from the PET image, and to then compute the change of the considered measure [17]. Among all tomographic medical imaging methods (ultrasound, CT, MR, and single photon emission computed tomography), FDG PET images have the best contrast for most cancers. Consequently, PET imaging is becoming more and more used for diagnosis purposes and to guide therapy [13]. However, the CT provides an accurate anatomical image and no PET-only scanners are manufactured for oncology imaging anymore [22]. Combined CT and PET scanning gives the precise localization of FDG uptake.

Among the large number of methods for estimating tumor change or tumor tracking, the following three approaches are the most popular:

- Analyzing the difference of images: this approach consists in analyzing the registration error between two images. One image is considered as the reference image and the second one is registered toward this reference. The

difference between the registered image and the reference image allows detecting tumor changes [10, 7]. Other methods based on differences between images have been proposed, in particular for brain tumors, using a statistical analysis of grey levels and contrast [1, 2].

- Analyzing the deformation field: as in the previous approach the registration of the images to a common reference is required. However, in this approach instead of working with the registration, the deformation field is analyzed to define tumor changes [20, 18].
- Sequential segmentation: this is the standard method to detect tumor change. The segmentation of the tumors is followed by a comparison of the segmented data to evaluate the tumor changes over time [9, 17, 23].

The two first approaches have the limitations inherent to registration methods. Indeed, spatial normalization of images in the presence of pathologies is still a very challenging problem. The registration algorithms are often based on the assumption of topological equivalence between the fixed and the mobile images. The presence of tumors in one image and not in the second one violates this assumption. Furthermore, the use of non-rigid registration can deform the tumor so much that the changes in the tumor cannot be detected in the difference map of images. The third approach is hampered by the difficulty to extract accurate target volumes. The estimation of tumor volume is still a very challenging problem. Note that Tylski [21] shows that tumor volumes can have opposite variations depending on the method used to estimate the tumor volume. Nevertheless, the methods discussed in this study are used in clinical practice [21].

While there are many studies of longitudinal tumor or lesion tracking in brain diseases such as Multiple Sclerosis (MS), there are few studies related to lung tumors. The lack of longitudinal tracking studies of lung tumors is due to the complexity of the deformation that the lung is undergoing during respiration, and the difference between the physical properties of the tumors and the lung tissue. Furthermore, the significant change of the tumor shape and appearance during long periods makes longitudinal tracking of lung tumors more challenging. An example is shown in Figure 1. Patient specific models based on mathematical models with parameters computed from the image data were proposed to describe the evolution of brain tumors in order to improve margins for radiotherapy [8]. Such models do not exist yet for image-based longitudinal tracking of lung tumor due to the complexity of lung and tumor deformations. In longitudinal tracking of lung tumors much effort has been dedicated to the development of techniques for segmentation, a follow up of the segmented data through time is then performed to detect tumor changes [7, 9, 17, 23].

In this paper we introduce a method for the longitudinal tracking of tumors that combines the advantages of the registration based and segmentation based approaches. Indeed the registration error is integrated in a temporal segmentation process using a new probabilistic framework. We propose a stochastic active model to incorporate prior knowledge about the evolution of the tumors from the previous CT images (or the current PET images if they are available) to constrain the tracking process in the current CT image. The model does not

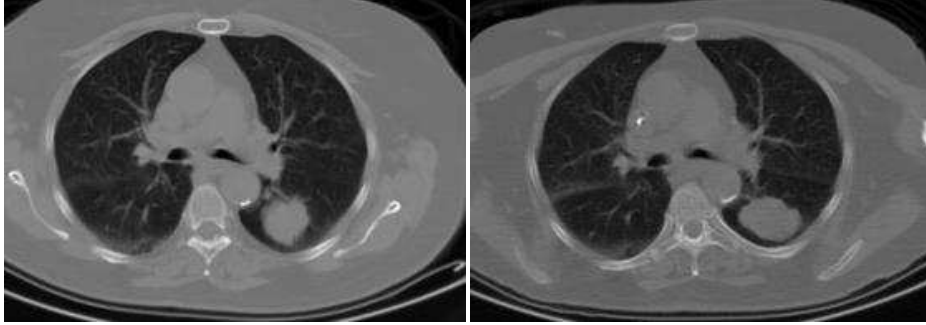


Fig. 1. Images of the same patient acquired in 2007 and in 2008.

require an initialization at each time point, only information given by the user from a reference image is needed. The information given by the user can be a segmentation of the tumor in the reference image or only two points, one point given inside the tumor and the second point on the tumor surface. This input is used as key points to construct a probabilistic function to constrain the evolution of level sets inside the image. One important aspect of our stochastic active contour is that it is flexible to allow the level sets to fit the boundary of the target tumor.

The first level set method with prior knowledge about shape was introduced by Leventon et al. [11]. Recent improvements of this approach were proposed in [5]. These methods are more adapted to segment structures with small changes in shape. However, the tumor shape does not at all respect this property: the same tumor can have different shapes between two longitudinal acquisitions. Tumors can shrink or grow over time, which can be reflected in CT-images in large changes of shape, appearance and volume. All these approaches use a Bayesian framework to constrain the evolution of the level sets.

Our approach introduces a new active contour using a different probabilistic framework, namely chance constraints [6]. Chance constraints programming (CCP) permits constraint violation up to a specified limit and ensures explicitly that the constraints will hold even with a high probability. In contrast, the Bayesian models do not ensure this latter characteristic of CCP models. They take into account information obtained through sampling and then formulate a decision problem. More generally, optimization under CCP is the unique probabilistic framework that ensures that constraints will hold with a high probability. The proposed CCP level set method allows us to incorporate a flexible prior using local and global confidence maps to weigh the evolution of the level set. The local confidence map corresponds to a voxel-wise registration error between the reference image and the target. The reference image is used to measure the evolution of the tumor in the studied images compared to this reference, it can be one of the images studied or an external template. The second confidence map corresponds to a α -quantile that regulates globally the evolution of the level set in the image. The whole process of our method is summarized into the following

three steps: (1) estimate the position and shape of the tumors in the reference image; (2) construct probabilistic constraints from the position estimated at the first step; (3) extract the tumors at each time point using the constraint defined in the second step.

In Section 2, we will give more details about each step and how to use it for longitudinal tracking in CT images. In Section 3 we adapt this approach to tumor tracking in CT/PET images, and in Section 4 we apply our approach on CT and CT/PET data.

2 Stochastic active contours for longitudinal segmentation of tumors

2.1 Chance-constrained level set method

Active contour models consist in evolving a curve (2D case) or surface (3D) constrained by image-based energy toward the target structure. Chan and Vese [4] proposed a region based model adapted to segment image with poor boundaries (edge information). This model is a piece-wise constant approximation of the Mumford and Shah functional [16]:

$$\mathcal{V}(\phi, c_1, c_2) = \int_{\Omega} \left(\lambda_1 (u_0 - c_1)^2 H_{\epsilon}(\phi) + \lambda_2 (u_0 - c_2)^2 (1 - H_{\epsilon}(\phi)) + \mu \delta_{\epsilon}(\phi) |\nabla \phi| + \nu H_{\epsilon}(\phi) \right) dx, \quad (1)$$

where Ω is the image domain; u_0 is a given image function; λ_1 , λ_2 , ν , and μ are positive parameters; c_1 and c_2 are two scalar constants used to separate the image into two regions of constant image intensities. The two last terms in the equation introduce regularization constraints, where H_{ϵ} and δ_{ϵ} are respectively the regularized Heaviside and Dirac functions, in this work they are approximated by:

$$H_{\epsilon}(\tau) = \frac{1}{2} \left(1 + \frac{2}{\pi} \text{artang}\left(\frac{\tau}{\epsilon}\right) \right); \quad \delta_{\epsilon}(\tau) = \frac{1}{\pi} \frac{\epsilon}{\epsilon^2 + \tau^2}. \quad (2)$$

While the Chan and Vese energy constraint introduces regularization to smooth the deformation and to deal with noise, it does not introduce a bias towards the target structure. Bayesian models were proposed in the literature to incorporate prior knowledge about the target structure to constrain the evolution of the level set [11]. These models are adapted to segment an object with well defined shape. However the tumor shape is undergoing large changes over long time periods and it is difficult to define a model that describes the evolution of tumors over time from image information. This makes the definition of an accurate prior for tumor tracking a very challenging problem that has led us to introduce chance constraints. Our approach consists in minimizing the Chan and Vese functional in the probabilistic admissible space:

$$\mathcal{A}_{1-\alpha} = \left\{ \phi : P(x, \phi) > 1 - \alpha, \text{ for almost all } x \in \Omega \right\}, \quad (3)$$

where P is a probabilistic constraint that introduces a priori information about the target from a given prior defined by the user from the reference image. Note

that the probabilistic constraint $P(x, \phi)$ is defined for each x in Ω , for simplicity we will note $P(\phi)$ instead of $P(x, \phi)$. The integration over the image domain Ω of P is done only in Equation (4). For high values of the probabilistic constraint the prior introduced by this function constrains the tracking process strongly whereas for small values the constraint is very weak. The α -quantile ($0 < \alpha < 1$) regulates the influence of these probabilistic constraints in the tracking process. In Section 4, we will see that α can be chosen in a large range for tumor tracking in CT and CT/PET images. In the next section we will present the methods used to construct the probabilistic constraints and how to apply it to tumor tracking. This model is flexible and adapted to follow tumors. The level set evolution is monitored by the local and global confidence maps that we have defined in the previous section.

We formulate our optimization approach using the penalization method, which is well adapted to stochastic optimization. The basic idea of the penalization method is to transform the constrained optimization problem into an unconstrained optimization problem:

$$E(\phi, c_1, c_2) = \mathcal{V}(\phi, c_1, c_2) + \rho \int_{\Omega} \max(0, 1 - \alpha - P(\phi))^2 \delta_{\epsilon}(\phi) dx, \quad (4)$$

where $\rho > 0$ is a penalty parameter¹; the δ_{ϵ} function allows us to restrict the shape prior within the region of interest. For ϕ constant, we deduce the values of c_1 and c_2 :

$$c_1(\phi) = \frac{\int_{\Omega} u_0 H_{\epsilon}(\phi) dx}{\int_{\Omega} H_{\epsilon}(\phi) dx}, \quad c_2(\phi) = \frac{\int_{\Omega} u_0 (1 - H_{\epsilon}(\phi)) dx}{\int_{\Omega} (1 - H_{\epsilon}(\phi)) dx} \quad (5)$$

As in [4] we use an artificial parameter t in the Euler-langrange formulation associated to Equation (4) :

$$\begin{aligned} \frac{\partial \phi}{\partial t} &= \left(\mu \operatorname{div} \left(\frac{\nabla \phi}{|\nabla \phi|} \right) - \nu - \lambda_1 (u_0 - c_1)^2 + \lambda_2 (u_0 - c_2)^2 \right) \delta_{\epsilon}(\phi) + \\ \rho \left(\max(0, 1 - \alpha - P(\phi)) \nabla P(\phi) \delta_{\epsilon}(\phi) + \max(1 - \alpha - P(\phi), 0)^2 \frac{\partial \delta_{\epsilon}}{\partial \phi}(\phi) \right) &= 0 \quad (6) \\ \text{in } \Omega \times \mathbb{R}^+; \phi(x, 0) = \phi_0(x) \text{ in } \Omega; \quad \frac{\delta_{\epsilon}(\phi)}{|\nabla \phi|} \frac{\partial \phi}{\partial n} &= 0 \text{ on } \partial \Omega \end{aligned}$$

The estimation of the solution of the model (4) can be summarized in the following steps:

- initialize $\phi = \phi_0$, $n = 0$;
- compute $c_1(\phi_n)$ and $c_2(\phi_n)$ by the relations (5);

¹ Note that if $\phi \in \mathcal{A}_{1-\alpha}$, the penalty is null whereas for $\phi \notin \mathcal{A}_{1-\alpha}$ a second term is added to the functional \mathcal{V} to introduce a penalty for violating the constraint $\phi \in \mathcal{A}_{1-\alpha}$.

- compute ϕ_{n+1} by solving the PDE (6) with respect to ϕ ;
- update periodically the level set ϕ_n by a signed distance;
- repeat the last two steps until convergence (ϕ_n is stationary).

The estimation of the probabilistic constraint P and its gradient will be discussed in Section 2.2.

2.2 Design of the probabilistic constraints

In this section we describe the method used to construct the probabilistic constraints that guide the evolution of our stochastic active contour. The method consists of the two following steps: (1) construct a deterministic prior; (2) construct the probabilistic constraints. In the first step we extract prior from the reference image. This prior can be a segmentation of the tumors from this reference image. The segmentation of each tumor corresponds to a surface which approximates the boundary of this tumor. The segmentation can be replaced by two points given by the user for each tumor, the first point is required to be inside the tumor and the second point on the tumor surface. These two points allow us to approximate the tumor boundary with a closed surface centered at the point chosen inside the tumor and with a radius defined by the second point. At the end of this first step we construct a set of surfaces, each surface approximates the boundary of one tumor in the reference image.

The aim of the second step is to build from these surfaces probability maps that we use to constrain the evolution of the level. We propose to use chance constraints [6], these constraints are defined from a set of random constraints. Each surface allows us to construct a component g_p of the random constraint such that the level set function ϕ satisfies:

$$g_p(\phi, \Lambda) \leq c_p, p = 1, \dots, n_t \quad (7)$$

where n_t is the number of tumors detected in the reference image and $c_p, p = 1, \dots, n_t$ are real constants; Λ is a random vector, with a multi-variate normal distribution, describing the uncertainty about the localization and the shape of the tumor boundary in the current image. As for P , for simplicity we noted $g(\phi, \lambda)$ instead of $g(x, \phi, \lambda)$. The argument x is given to the constraints g_p via ϕ and the registration error. An example of random constraints is given in by Equation (15) in Section 2.4. We can picture each component of the random constraint as a surface that oscillates around the boundary of one tumor in the reference image. The oscillations are monitored by the random vector Λ , the dimension of Λ corresponds to the number of tumors in the reference image and the covariance matrix is estimated from the registration errors of the reference image and each target image. The registration error is computed before the evolution of the levels and is used as confidence map in the stochastic term. Locally, the level set follows the target image in regions with a high voxel-wise registration error while it follows the prior in regions with low voxel-wise registration errors. The global confidence map corresponds to a α -quantile such that:

$$P(\phi) = \mathbb{P}\left(g_p(\phi, \Lambda) \leq c_p, p = 1, \dots, n_t\right) > 1 - \alpha. \quad (8)$$

The α -quantile is used to monitor the evolution of the level set according to the random constraints (7): the model allows the active contour to evolve towards regions that violate the constraint for a small amount of realizations when no alternative solution is found. For a large α the level set follows the data while for small α the level set follows the prior. The α -quantile is given by the user to introduce his knowledge about the evolution of tumors in the studied images. This parameter can be also estimated from the registration error, when the registration error is small we can introduce a strong prior from the reference image to constrain the tracking process. Moreover, we will show in Section 4 that the parameter α can be chosen in a large range. In this method we have used the rigid registration, this choice will be discussed in Section 2.4. In Section 2.4, we will give an example of probabilistic constraints that can be used to track a single tumor. In this case the estimation of the probabilistic constraint and its gradient is computed analytically. Figure 2 shows examples of the probabilistic constraints. However, in the case of more than one tumor or when several random constraints are needed, the probabilistic constraint can be intractable analytically. In the next section, we will discuss how the probabilistic constraints and their derivatives can be computed in this situation.

2.3 Estimation of the probabilistic constraint and its derivative

In this section we present the method used to estimate the probabilistic constraint, described in the previous section, and its derivative. If the random constraints are nonlinear, to compute the gradient we need to perform the following approximation:

$$g_p(\phi, A) \simeq g_p(\phi, 0) + \sum_{q=1}^{n_t} \frac{\partial g_p}{\partial \Lambda_q}(\phi, 0) \Lambda_q,$$

for random variables Λ_q , $q = 1 \dots n_t$ with zero means and small variances. Therefore the probability $P(\phi)$ in relation (8) can be approximated by:

$$P(\phi) = \mathbb{P}\left(G(\phi) A \leq C(\phi)\right), \quad (9)$$

where :

$$G_{pq}(\phi) = \frac{\partial g_p}{\partial \Lambda_q}(\phi, 0), \quad p = 1, \dots, n_t, \quad q = 1, \dots, n_t \quad (10)$$

$$C_p(\phi) = c_p - g_p(\phi, 0), \quad p = 1, \dots, n_t. \quad (11)$$

Since A has a zero mean multi-variate distribution, the random vector $G(\phi)A$ has also a zero mean multi-variate normal distribution with the covariance matrix:

$$\Gamma(\phi) = G(\phi)KG(\phi)^t,$$

where K is the covariance matrix of A .

The probability $P(\phi)$ can be expressed as the n_t -dimensional integral :

$$P(\phi) = \int_{-\infty}^{C_1(\phi)} \cdots \int_{-\infty}^{C_{n_t}(\phi)} p_{\Gamma(\phi)}(z_1, \dots, z_{n_t}) dz_1 \cdots dz_{n_t},$$

where p_{Γ} is the density of the n_t -dimensional normal distribution with a zero mean and a covariance matrix Γ :

$$p_{\Gamma}(z) = \frac{1}{\sqrt{(2\pi)^{n_t} \det(\Gamma)}} \exp\left(-\frac{1}{2} z^t \Gamma^{-1} z\right).$$

The gradient of $P(\phi)$ is given by the relation:

$$\nabla P(\phi) = \sum_{i,j=1}^n A_{ij}(\phi) \frac{\partial \Gamma_{ij}}{\partial \phi} + \sum_{i=1}^n B_i(\phi) \frac{\partial C_i}{\partial \phi} \quad (12)$$

where the matrix A and the vector B are given by:

$$\begin{aligned} A_{ij}(\phi) &= \int_{-\infty}^{C_1(\phi)} \cdots \int_{-\infty}^{C_n(\phi)} \frac{\partial p_{\Gamma}}{\partial \Gamma_{ij}}(z_1, \dots, z_n) dz_1 \cdots dz_n \Big|_{\Gamma=\Gamma(\phi)} \\ &= \int_{-\infty}^{C_1(\phi)} \cdots \int_{-\infty}^{C_n(\phi)} \frac{\partial \ln p_{\Gamma}}{\partial \Gamma_{ij}}(z) p_{\Gamma}(z) d^n z \Big|_{\Gamma=\Gamma(\phi)}, \end{aligned} \quad (13)$$

$$\begin{aligned} B_i(\phi) &= \int_{-\infty}^{C_1(\phi)} \cdots \int_{-\infty}^{C_{i-1}(\phi)} \int_{-\infty}^{C_{i+1}(\phi)} \cdots \int_{-\infty}^{C_n(\phi)} \\ &\quad \times p_{\Gamma(x)}(z_1, \dots, z_i = C_i(x), \dots, z_n) dz_1 \cdots dz_{i-1} dz_{i+1} \cdots dz_n \\ &= \frac{1}{\sqrt{2\pi \Gamma_{ii}}} \exp\left(-\frac{C_i(\phi)^2}{2\Gamma_{ii}}\right) \int_{-\infty}^{C_1(\phi)} \cdots \int_{-\infty}^{C_{i-1}(\phi)} \int_{-\infty}^{C_{i+1}(\phi)} \cdots \int_{-\infty}^{C_n(\phi)} \\ &\quad \times p_{\Gamma(x)}(z' | z_i = C_i(\phi)) d^{n-1} z'. \end{aligned} \quad (14)$$

Here $p_{\Gamma}(z' | z_i)$ is the conditional density of the $(n_t - 1)$ -dimensional random vector $Z' = (Z_1, \dots, Z_{i-1}, Z_{i+1}, \dots, Z_{n_t})$ given $Z_i = z_i$. Therefore, $p_{\Gamma}(z' | z_i = C_i(\phi))$ is the density (n_t-1) -dimensional normal distribution with mean:

$$\tilde{\mu}^{(i)} = \left(\frac{C_i(\phi) \Gamma_{ji}(\phi)}{\Gamma_{ii}} \right)_{j=1, \dots, i-1, i+1, \dots, n_t}$$

and $(n_t - 1) \times (n_t - 1)$ covariance matrix

$$\tilde{\Gamma}^{(i)} = \left(\Gamma_{kl} - \frac{1}{\Gamma_{ii}} \Gamma_{ki} \Gamma_{il} \right)_{k,l=1, \dots, i-1, i+1, \dots, n_t}.$$

We give in [6] an efficient Monte Carlo estimation of the functions $A_{ij}(\phi)$ and $B_i(\phi)$. Note that if Γ is diagonal, then the gradient of $P(\phi)$ is given by the relation:

$$\nabla P(\phi) = \sum_{p=1}^{n_t} \frac{\frac{\partial C_p}{\partial \phi} \Gamma_{pp}(\phi) - \frac{1}{2} C_p(\phi) \frac{\Gamma_{pp}}{\partial \phi}}{\Gamma_{pp}(\phi)^{3/2}} \Phi' \left(\frac{C_p(\phi)}{\sqrt{\Gamma_{pp}(\phi)}} \right)$$

where Φ' is the derivative of the standard normal distribution function. Note that in the case of a single constraint the estimation of the probabilistic constraint and its gradient is computed analytically, see next section.

2.4 Probabilistic constraint for a single tumor

In this section we describe the process used in this work to construct an explicit random constraint to define the prior that will constrain the tracking process. As explained in Section 2.2, for each tumor we generate from the user input a surface \mathcal{S} that approximates the tumor boundary in the reference image. Let $\tilde{\phi}$ be defined as the signed distance associated with the surface \mathcal{S} :

$$\tilde{\phi}(x) = \begin{cases} D(x), & \text{if } x \text{ is inside } \mathcal{S}, \\ -D(x), & \text{otherwise,} \end{cases}$$

where D is a distance from \mathcal{S} : $D(x) = \inf_{y \in \mathcal{S}} d(x, \mathcal{S})$ with d a given metric, we use in this work the Euclidean metric. We consider the following random constraint:

$$g(\phi, \Lambda) = e\Lambda + (\phi - \tilde{\phi})^2 \leq 0. \quad (15)$$

where e is the confidence map and Λ is a random variable with a Gaussian distribution with the variance σ^2 . Consequently the random variable $\mathcal{Y} = e\Lambda$ has a Gaussian distribution with the variance $(e\sigma)^2$ and with the normal distribution $p_{\mathcal{Y}}$. Consequently, the probabilistic constraint P , given by Equation (8), becomes:

$$P(\phi) = \int_{-\infty}^{-(\tilde{\phi}-\phi)^2} p_{\mathcal{Y}}(z) dz = \frac{1}{2} \left(1 + \operatorname{erf} \left(\frac{-(\phi - \tilde{\phi})^2}{e\sigma\sqrt{2}} \right) \right). \quad (16)$$

where erf is the Gauss error function². Note that the level set function ϕ is very close to the prior $\tilde{\phi}$ when P is close to its maximum value 0.5. This probability is the one used in Equation (4). Figure 2 shows examples of the probabilistic constraint $\phi \rightarrow \mathbb{P}(g(\phi, \Lambda) \leq 0)$ associated with the random constraint (15). We have considered two examples of the confidence map, in the first example $e \equiv \mathbf{1}$ ($x \rightarrow e(x) = 1, \forall x \in \mathbb{R}^3$), and in the second example we defined e as a voxel-wise registration error plus a very small strictly positive constant. The registration was performed with rigid transformation. We will discuss this choice in the next section.

2.5 Local confidence map

In this section, we will compare confidence maps (registration errors) computed with the following registration methods: Rigid, Affine, B-Spline, and Demons using the correlation coefficient as a similarity measure. Figure 3 shows registration results obtained with these methods and the registration errors. In a second

² $\operatorname{erf}(x) = \frac{2}{\sqrt{\pi}} \int_0^x \exp(-t^2) dt$

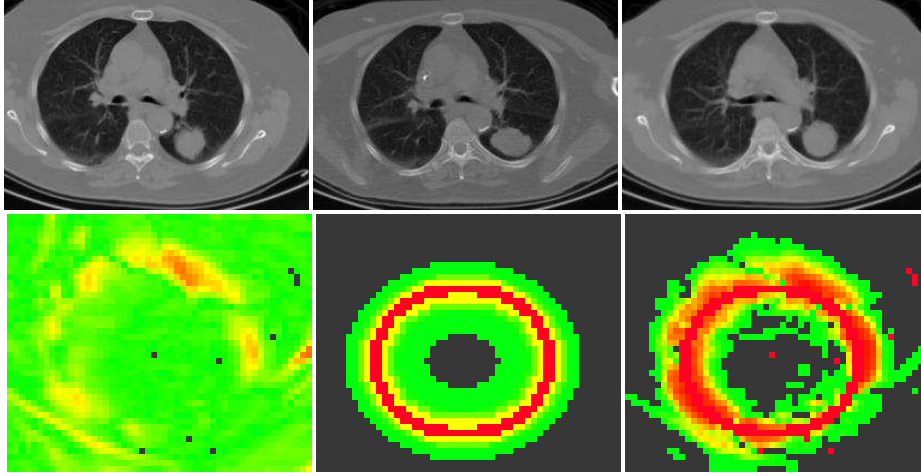


Fig. 2. Confidence map. First row, left: image acquired in 2007 (mobile image); center: image acquired in 2008; right: registered image using rigid transformation. Second row, the left panel shows the registration error (ROI on the tumor); the center panel shows the probabilistic constraint computed without registration error; the right panel shows the confidence map computed using the registration error. The red color corresponds to high values, the yellow to medium values, and green to low values.

experiment we have segmented the lungs from all images and performed an intensity registration of the segmented data, see Figure 4. To compare the registration quality, we have considered three metrics: mean squares (MS), normalized correlation (CC), and normalized correlation coefficient histogram (CCH). These metrics are calculated with the following relations:

$$MS(I_f, I_m) = \frac{1}{N} \sum_{i=1}^N (I_f(x_i) - I_m(x_i))^2 \quad (17)$$

$$CC(I_f, I_m) = \frac{\sum_{i=1}^N I_f(x_i) I_m(x_i)}{\sqrt{\sum_{i=1}^N I_f^2(x_i) \sum_{i=1}^N I_m^2(x_i)}} \quad (18)$$

$$CCH(I_f, I_m) = \frac{\sum_{f,m} H(f, m)(I_f I_m - \bar{I}_f \bar{I}_m)}{\sum_f H(f)(I_f - \bar{I}_f)^2 \sum_m H(m)(I_m - \bar{I}_m)^2} \quad (19)$$

where I_f and I_m are respectively the fixed image and the transformed image, N is the number of pixels in the images I_f and I_m ; the values \bar{I}_f and \bar{I}_m are the mean values of I_f and I_m ; $H(f, m)$ is the joint histogram of I_f and I_m ; $H(f)$

and $H(m)$ are respectively the histogram counts of I_f and I_m . The transformed image is obtained by mapping the mobile image with the transformation computed by registering the mobile image to the fixed image. The comparison of the registration errors in terms of the metrics, MS, CC, and CCH is presented in Table 1. On the one hand, the B-Spline method gives the smallest registration error according to the three metrics. Furthermore, these results can be improved by increasing the number of control points in the B-Spline method. On the other hand the B-Spline method deforms the tumor so much that the change in the tumor is not well detected in the difference image, which is defined as the absolute value of the the difference between the fixed and the transformed image. To deal with this problem, the authors in [12, 19, 15, 14] proposed to constrain the control points located on the tumor to have a rigid deformation during the registration process. While this approach allows preserving the tumor volume, it requires the segmentation of the tumor to define the rigid constraints. Therefore, we have chosen the rigid registration to compute the confidence map which is used to construct the probabilistic constraints for our stochastic level set method.

Registration method	Not segmented data			Using segmented lungs		
	SM	CC	CCH	SM	CC	CCH
Rigid	050724.5	0.831	0.777	53394.10	0.842	0.774
Affine	069959.9	0.801	0.735	64196.10	0.816	0.737
B-Spline	037430.4	0.868	0.829	09788.99	0.963	0.948
Demons	105160.0	0.729	0.630	82955.60	0.783	0.688

Table 1. Comparison of the following registration methods: Rigid, Affine, B-Spline, and Demons with respect to the metrics SM, CC, and CCH.

2.6 Chance-Constrained Programming versus Bayesian model

In this section we compare the proposed approach with the traditional approach of introducing shape priors in the level set formulation: the Bayesian model. In the formulation (15), we introduce as a probabilistic constraint that the similarity between ϕ and $\tilde{\phi}$ is superior to a given quantile. In the Bayesian formulation the prior is introduced through sampling and then a decision problem is formulated. To compare our CCP level set method with the Bayesian level set model, we developed a Bayesian approach that can be compared to the CCP model proposed in this paper. Let $\mathbb{P}(\phi|\tilde{\phi}, u)$ be the posterior probability of the level set ϕ given the image function u and the level set shape prior $\tilde{\phi}$ defined in the previous section. The Bayesian formulation of this probability is given by Bayes' theorem:

$$\mathbb{P}(\phi|\tilde{\phi}, u) = \frac{\mathbb{P}(\tilde{\phi}, u|\phi) \mathbb{P}(\phi)}{\mathbb{P}(\tilde{\phi}, u)} \propto \mathbb{P}(\tilde{\phi}|\phi) \mathbb{P}(u|\phi) \mathbb{P}(\phi) \quad (20)$$

where $\mathbb{P}(\tilde{\phi}|\phi)$ is the shape prior term. We suppose that this probability follows a Gaussian distribution and that $\mathbb{P}(u|\phi) \mathbb{P}(\phi)$ is derived from the Chan and

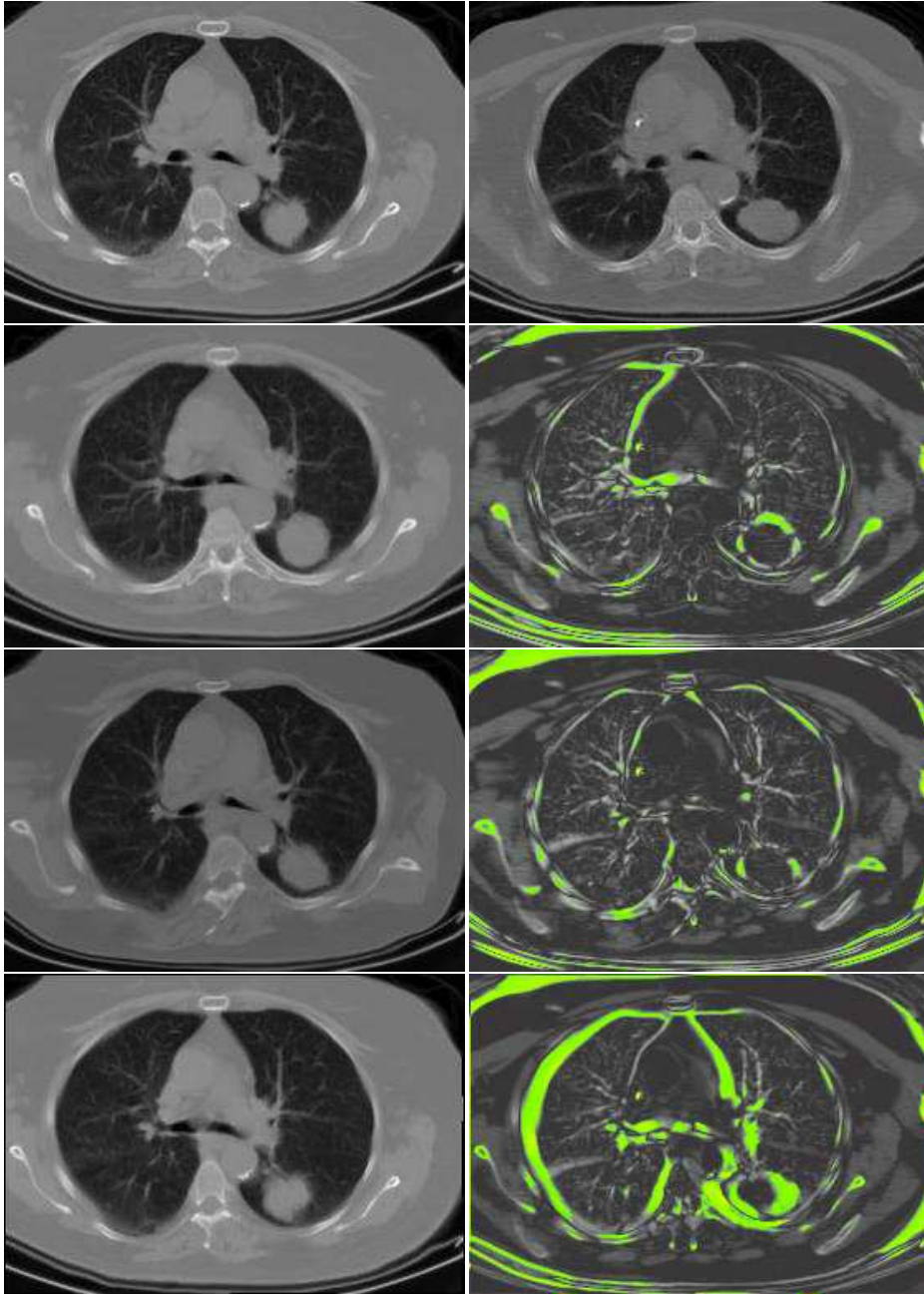


Fig. 3. First row, left: image acquired in 2007 (mobile image); right: image acquired in 2008. In the second, third and fourth rows, on the left the registered image using rigid, B-Spline, and Demons methods, respectively; on the right, the registration errors for each registration method. The green color correspond to high values of the registration error.

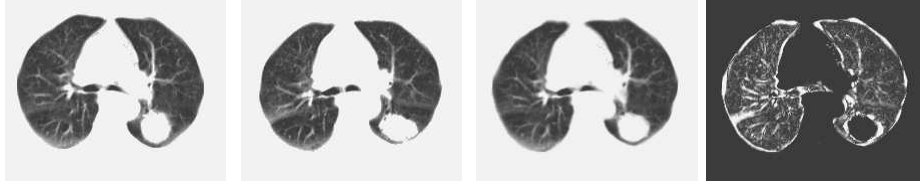


Fig. 4. B-Spline registration with segmented lungs. First panel, segmentation of the image acquired in 2007; second panel, segmentation of the image acquired in 2008; third panel, the registered image; fourth panel, the registration error.

Vese model, see Equation (1). Therefore, the maximum of the posterior probability (20) is equivalent to the lowest energy of the $-\log$ functional, and after integration over the image domain we end up with the following Bayesian model:

$$E_b(\phi, c_1, c_2) = \mathcal{V}(\phi, c_1, c_2) + \gamma \int_{\Omega} \frac{(\phi - \tilde{\phi})^2}{2\sigma^2} dx \quad (21)$$

where γ is a weight parameter on the prior. We will see in the result section how this parameter affects the segmentation results in the Bayesian and CCP level set methods.

Formally, comparing Equations 21 and 4, it is clear that in the Bayesian model, the penalty depends continuously on the distance between ϕ and $\tilde{\phi}$, averaging over all points of Ω , while CCP is able to accommodate constraint violation up to a controlled extent, in a globally satisfied constraint, guaranteed with a high probability (see also the discussion below).

3 Longitudinal tracking in CT/PET

In this section we adapt the previous method which was developed for CT-tracking to multi-modality CT/PET.

The segmentation of tumors using a simple threshold of the PET images is still a matter of debate [3]. Here we used a PET threshold of 30% to 50% as a first approximation of the tumor boundary that we use to construct the probabilistic constraint as described in Section 2.4. Subsequently, we perform a longitudinal tracking of the tumors in the CT images with these probabilistic constraints using our stochastic level set method presented in Section 2.1. The tracking process in CT/PET can be summarized as follows:

1. Threshold the PET image at the time point t between 30% and 50% in such a way that each tumor corresponds to only one connected component. Morphological filtering may be needed to ensure this property.
2. Construct from the approximation of the tumor boundary, obtained in the first step, the probabilistic constraint according to the method presented in Section 2.2.

3. Perform the stochastic level set method in CT image at the time point t according to the process (6).
4. Get the CT/PET image at time $t + 1$ and go to step (1).

Note that the use of the multi-modality CT/PET helps us to reduce the intervention of the user in the tracking process. In CT/PET only a single point given by the user on the target tumor is needed. Furthermore, in CT/PET the probabilistic constraint is used with high confidence compared to the probabilistic constraint used for the tracking with CT data only. Indeed, the prior used for CT-stochastic tracking is computed from a reference image acquired at a different date whereas in CT/PET-stochastic tracking the prior is computed from the PET image acquired at the same date as the CT image.

4 Results

The data are composed of two data sets for two patients and each data set is composed of at least two images acquired at different time points: for patient 1, data were acquired on 02/2007 and 03/2008 and for patient 2 on 06/11/2007, 05/14/2008, and 07/24/2008. The CT and PET resolutions are $1.172 \times 1.172 \times 5 \text{ mm}^3$ and $4 \times 4 \times 4 \text{ mm}^3$, respectively. For the CT scan, the patients held their breath at full inspiration during the acquisition.

We have applied our stochastic model to track tumors in CT and CT/PET images. For the CT data, the level set function that is used as prior to constrain the tracking process is constructed from the image acquired at the first date. The tracking process is performed with the images acquired at the following dates, which are used as fixed images in the registration process. For the CT/PET images, we used the PET threshold between 30% and 50% as a first approximation of the tumor boundary that we use to construct the probabilistic constraint as described in Section 2.2. The longitudinal segmentation is performed in the CT image acquired as the same date as the PET image used to build the constraints. Figure 6-second-row shows the results obtained for patient 1 with our stochastic active contour model using only the CT scan. Figure 6-first-row(right) shows the results obtained using the CT/PET data. Figure 7-center shows a comparison between the manual segmentation and the results obtained with our CCP level set method using different values of α , the best results were obtained with $0.6 < \alpha < 0.85$. This shows also that the quatile α can be chosen for CT and CT/PET longitudinal segmentation in a large range. For α smaller than 0.6 the probabilistic constraint constrains strongly the segmentation process, as we can see in Figure 6-second-row the results are very close to the level set prior, whereas for α superior to 0.8 the constraint is very weak, therefore the propagation leaks outside the region of interest (localization of the tumor).

In Table 2, we compare the results obtained with our CCP level set method and the Bayesian model using the CT and CT/PET data for the two patients. Note that only manual segmentations were available for the CT images, this may explain the relatively low values of the Dice measure for the CT/PET

segmentation. Figure 7 compares the two approaches using different values of the parameters that weight on the prior for each approach. The CCP model gives the best results in terms of Dice measure. For the two patients considered in this study, a strong prior leads to an underestimation of the area of the tumor for both models. However, in contrast to the CCP model the Bayesian model suddenly leaks outside the tumor when a weak or medium weight on the prior is used. This can be explained by the fact that the prior in the CCP model is introduced as an explicit constraint which allows us to constrain the segmentation more efficiently.

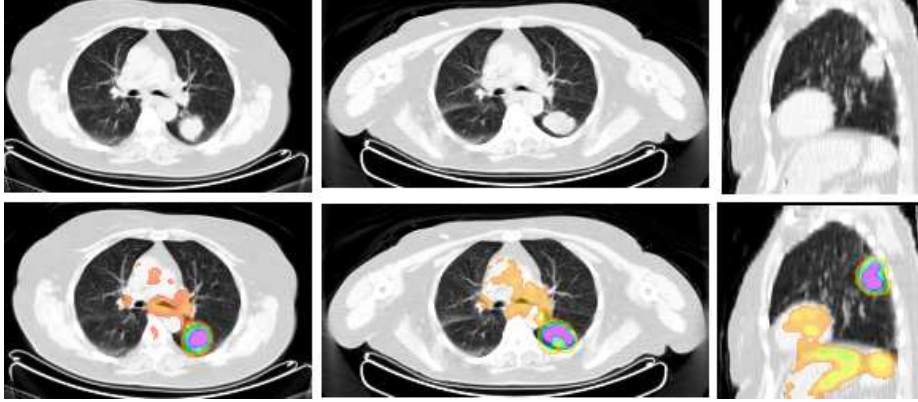


Fig. 5. CT and CT/PET images of the same time acquired in 2007 and 2008. First row, left: the CT image acquired in 2007; center and right: CT image acquired in 2008. Second row, left: PET image overlaped with the CT image acquired in 2007; center and right: PET image overlaped with the CT image acquired in 2008.

Patient	Modality	Dice similarity		Sensitivity		Specificity	
		CCP	BAY	CCP	BAY	CCP	BAY
1	CT	0.898	0.851	0.815	0.774	1.000	0.945
1	CT/PET	0.772	0.723	0.653	0.585	0.944	0.945
2	CT	0.875	0.826	0.784	0.705	0.991	0.996
2	CT/PET	0.806	0.700	0.678	0.539	0.994	0.997

Table 2. Comparison of the proposed CCP level set method with the Bayesian model in terms of the following evaluation measures: Dice similarity, sensitivity and specificity, using CT and CT/PET data for two patients.

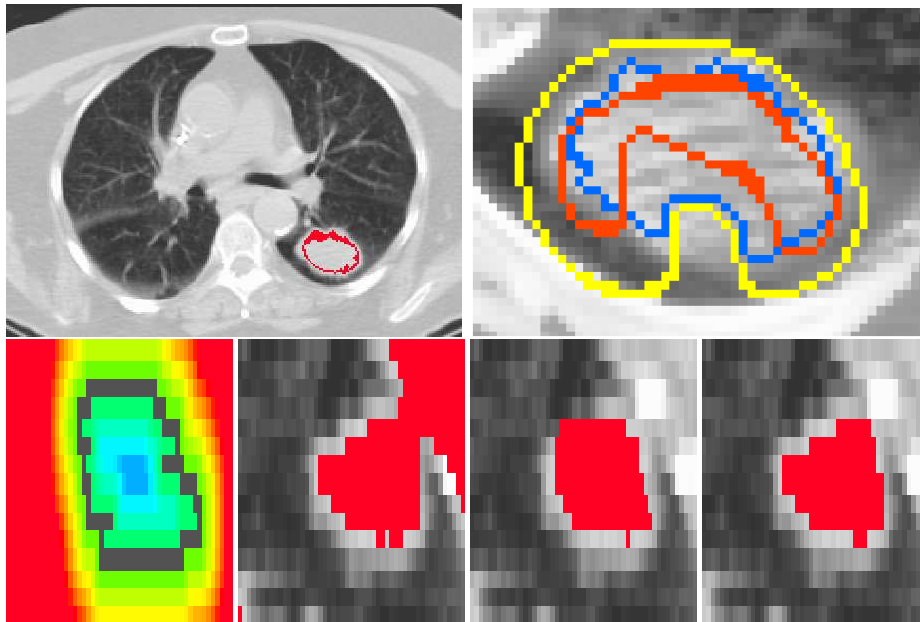


Fig. 6. 3D longitudinal segmentation of tumors with our CCP level set method in CT and CT/PET. First row, left: the results obtained using only the CT images; right panel shows in blue the result obtained with our stochastic model, in yellow and red the PET level thresholded at 20% and 50% respectively. Second row, right panel: the signed distance from the initial contour (prior), the level zero of this distance corresponds to the black contour; the second panel shows the results obtained with $\alpha = 1$ (no prior); the third panel corresponds to $\alpha = 0.47$ (very strong prior); the right panel corresponds to $\alpha = 0.7$ (medium prior). See Figure 5 to locate the position of this lung tumor in 2007 and 2008.

5 Discussion and conclusion

We presented a novel approach for the longitudinal tracking of tumor in CT and CT/PET images. Our approach combines the registration and segmentation to derive a model that benefits from the advantages of each approach. We introduce chance constraints to incorporate priors for the shape and localization of the tumors. In the case of CT-tracking, the prior is computed from the registration error and the user input. In the case of CT/PET-tracking the prior is computed from the CT-registration error and by thresholding the PET images. Our results illustrate the efficiency and the flexibility of our approach: the method is adapted to large changes in tumor shape and the user can introduce priors easily from different sources. The prior is used to build chance constraints to guide the evolution of the level set in the CT images. The CCP makes it possible to introduce an explicit constraint and permits the violation of the constraints up to a specified level. However, the constraints can be hold even with high probability.

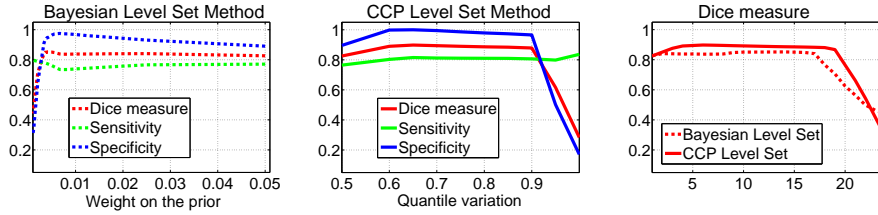


Fig. 7. CCP level set method versus Bayesian level set model. The left and middle panel show the effect of the variation on the prior parameters for CCP and Bayesian level set methods on the statistics: Dice similarity, Sensitivity, and Specificity; the right panel shows the variation of the Dice measure for the CCP and Bayesian level set methods.

On the one hand, the deterministic approach is too rigid to allow constraint violations. Therefore a solution that satisfies the constraint everywhere except for a very small set of image points will be rejected even when this solution gives the best minimizer except for this insignificant set of points. On the other hand the Bayesian models which introduce priors through sampling and then formulate a decision problem do not ensure that the constraint holds with a high probability. This makes chance-constrained programming a powerful and unique tool for optimization problems under uncertainty. CCP is therefore very suitable for medical image analysis where uncertainties and risk are omnipresent. In the future, we will validate the proposed approach using a larger data set.

References

1. E. D. Angelini, J. Atif, J. Delon, E. Mandonnet, H. Duffau, and L. Capelle. Detection of glioma evolution on longitudinal MRI studies. In *International Symposium on Biomedical Imaging (ISBI)*, pages 49–52, 2007.
2. E. D. Angelini, J. Delon, L. Capelle, and E. Mandonnet. Contrast mapping and statistical testing for low-grade glioma growth quantification on brain MRI. In *International Symposium on Biomedical Imaging (ISBI)*, pages 872–875, Rotterdam, The Netherlands, April 2010.
3. Q. C. Black, I. S. Grills, L. L. Kestin, C-Y O. Wong, J. W. Wong, A. A. Martinez, and i Yan. Defining a radiotherapy target with positron emission tomography. *International Journal of Radiation Oncology, Biology, Physics*, 60(4):1272–1282, November 2010.
4. T. F. Chan and L. A. Vese. Active contours without edges. *IEEE Transactions on Medical Imaging*, 10(2):266–277, 2001.
5. D. Cremers, M. Rousson, and R. Deriche. A review of statistical approaches to level set segmentation: Integrating color, texture, motion and shape. *International Journal of Computer Vision*, 72:195–215, 2007.
6. J. Garnier, A. Omrane, and Y. Rouchdy. Asymptotic formulas for the derivatives of probability functions and their Monte Carlo estimations. *European Journal of Operational Research*, 198(3):848–858, 2009.
7. Y. Kawata, N. Niki, H. Omatsu, M.Kusumoto, R. Kakinuma, K. Mori, H. Nishiyama andK. Eguchi, M. Kaneko, and N. Moriyama. Tracking interval

- changes of pulmonary nodules using a sequence of three-dimensional thoracic images. In *Medical Imaging 2000: Image Processing*, volume SPIE 3979, pages 86–96, 2000.
8. E. Konukoglu, O. Clatz, P. Bondiau, H. Delingette, and N. Ayache. Extrapolating tumor invasion margins for physiologically determined radiotherapy regions. In *MICCAI (1)*, pages 338–346, 2006.
 9. J. W. Kostis, P. A. Reeves, F. D. Yankelevitz, and I. C. Henschke. Three-dimensional segmentation and growth-rate estimation of small pulmonary nodules in helical CT images. *IEEE Transactions on Medical Imaging*, 22(10):1259–1274, oct. 2003.
 10. L. Lemieux, U. C. Wiesmann, N. F. Moran, D. R. Fish, and S. D. Shorvon. The detection and significance of subtle changes in mixed-signal brain lesions by serial MRI scan matching and spatial normalization. *Medical Image Analysis*, 2(3):227–242, 1998.
 11. M. E. Leventon, O. D. Faugeras, W. E. L. Grimson, and W. E. Wells III. Level set based segmentation with intensity and curvature prior. In *MMBIA*, pages 4–11, 2000.
 12. J. A. Little, D. L. G. Hill, and D. J. Hawkes. Deformations incorporating rigid structures. In *MMBIA*, page 104, Washington, DC, USA, 1996.
 13. D. A. Mankoff, F. O’Sullivan, W. E. Barlow, and K. A. Krohn. Molecular imaging research in the outcomes era: measuring outcomes for individualized cancer therapy. *Academic Radiology*, 14(4):398–405, 2007.
 14. A. Moreno, S. Chambon, A. Santhanam, J. Rolland, E. Angelini, and I. Bloch. Combining a Breathing Model and Tumor-Specific Rigidity Constraints for Registration of CT-PET Thoracic Data. *Computer Aided Surgery*, 13(5):281–298, September 2008.
 15. A. Moreno, G. Delso, O. Camara, and I. Bloch. Non-linear registration between 3d images including rigid objects: Application to CT and PET lung images with tumors. In *Workshop on Image Registration in Deformable Environments (DEFORM’06)*, pages 31–40, Edinburgh, UK, September 2006.
 16. D. Mumford and J. Shah. Optimal approximations by piecewise smooth functions and associated variational problems. *Communications on Pure and Applied Mathematics*, 42(5):577–685, 1989.
 17. A. P. Reeves, A. B. Chan, D. F. Yankelevitz, C. I. Henschke, B. Kressler, and W. J. Kostis. On measuring the change in size of pulmonary nodules. *IEEE Transactions on Medical Imaging*, 25(4):435–450, 2006.
 18. D. Rey, G. Subsol, H. Delingette, and N. Ayache. Automatic detection and segmentation of evolving processes in 3D medical images: Application to multiple sclerosis. *Medical Image Analysis*, 6(2):163–179, June 2002.
 19. C. Tanner, J. A. Schnabel, D. Chung, M. J. Clarkson, D. Rueckert, D. L. G. Hill, and D. J. Hawkes. Volume and shape preservation of enhancing lesions when applying non-rigid registration to a time series of contrast enhancing MR breast images. In *MICCAI*, pages 327–337, London, UK, 2000. Springer-Verlag.
 20. J. Thirion and G. Calmon. Deformation analysis to detect and quantify active lesions in 3D medical image sequences. *IEEE Transactions on Medical Imaging*, 18(5):429–441, 1999.
 21. P. Tylski, M. Dusart, B. Vanderlinden, and I. Buvat. Assigning statistical significance to tumor changes in patient monitoring using FDG PET. In *ISBI*, pages 121–124, 2008.
 22. R. L. Wahl. Why nearly all PET of abdominal and pelvic cancers will be performed as PET/CT. *Journal of Nuclear Medicine*, 45(1):82S–95S, 2004.

23. B. Zhao, L. H Schwartz, C. S. Moskowitz, M. S. Ginsberg, N. A. Rizvi, and M. G. Kris. Lung cancer: computerized quantification of tumor response—initial results. *Radiology*, 241:892–898, 2006.

